FDTD METHOD INVESTIGATION ON THE POLARIMETRIC SCATTERING FROM 2-D ROUGH SURFACE

J. Li, L.-X. Guo, and H. Zeng

School of Science
Xidian University
No. 2, Taibai Road, Xi'an, Shaanxi, China

Abstract—A polarimetric scattering from two-dimensional (2-D) rough surface is presented by the finite-difference time-domain (FDTD) algorithm. The FDTD calculations with sinusoidal and pulsed plane wave excitations are performed. As the sinusoidal FDTD is concerned, it is convenient to obtain the scattered angular distribution of normalized radar cross section (NRCS) from rough surface for a single frequency. And the advantage of pulsed FDTD is to calculate the frequency distribution of NRCS from rough surface in a scattered direction of interest. A single frequency scattering from rough surface by sinusoidal FDTD is validated by the result of Kirchhoff Approximation (KA). And the frequency response of rough surface by pulsed FDTD is verified by that of sinusoidal FDTD, which requires an individual FDTD run for every frequency. To save computation time, the MPI-based parallel FDTD method is adopted. And the computation time of parallel FDTD algorithm is dramatically reduced compared to a single-process implementation. Finally, the polarimetric scattering of rough surface with the sinusoidal and pulsed FDTD illumination are presented and analyzed for different polarizations.

1. INTRODUCTION

In recent years, the problem of studying the statistical properties of electromagnetic scattering from random rough interface has attached considerable interest in the fields of radar surveillance, surface physics, and remote sensing of ocean and soil. Usually the radar cross section (RCS) of rough surface is calculated and analyzed for different conditions. The electromagnetic scattering from one-dimensional (1-D) and two-dimensional (2-D) rough surface at a certain

Corresponding author: J. Li (lijuan029@yeah.net).

frequency has been extensively investigated by several methods. Some analytical approaches are the Kirchhoff approximation, the small slope approximation [1], the ray-tracing method [2], the extended boundary condition [3]. However, these approximate methods have restricted regions of validity in terms of slope and roughness of surface. So some numerical approaches are employed, which include the forward-backward method [4], the steepest descent-fast multipole [5], and the multilevel sparse-matrix canonical-grid method [6], etc. However, the complete RCS signature of a rough surface also includes the calculation of its frequency response. And only a few papers report this scattering characteristic of rough surface [7, 8].

In this paper, the finite difference time domain (FDTD) algorithm is utilized to investigate the polarimetric scattering of 2-D rough surface. To obtain the complete scattering characteristic of rough surface, the application of FDTD method in two areas is outlined. In steady state (only one frequency), one is interested in the distant scattering of rough surface in various scattered directions; In transient state, one desires the wide frequency response of rough surface in a scattered direction of interest. The former is usually solved by FDTD method with sinusoidal wave illumination (sinusoidal FDTD). It is convenient for the sinusoidal FDTD to obtain the RCS versus the scattered angle at a certain frequency by a FDTD run. In our previous work, this method has been utilized to solve the scattering from a randomly rough surface [9, 10] and the composite scattering from a target above a rough surface [11–13]. And the latter is achieved by the FDTD method with a pulsed plane wave excitation (pulsed FDTD). The advantage of the pulse FDTD is to calculate the RCS versus the frequency in a certain scattered direction by a FDTD run, even for the scattering from the frequency-dependent rough surface.

However, it is extremely time-consuming to compute the scattering from a 2-D large-scale rough surface using a single-process FDTD algorithm, since the unknowns of 2-D rough surface become extremely enormous with the increase of computation domain. To overcome the problem, a parallel-processing FDTD technique using the Message-Passing Interface (MPI) library [14] is employed in this paper.

The paper is organized as follows: The theoretical formulae of calculating scattering fields from 2-D rough surface by FDTD with sinusoidal and pulsed excitations are developed. And then the information about the parallel FDTD algorithm is introduced. Moreover, the NRCS of 2-D rough surface with sinusoidal and pulsed excitations for different polarizations are presented and analyzed in detail.

2. POLARIMETRIC SCATTERING FROM 2-D ROUGH SURFACE

In Figure 1, an incident wave is impinging on the 2-D Gaussian rough surface in the direction of $\mathbf{k_i}$, which makes angles θ_i relative to the z-axis, and ϕ_i relative to the x-axis. The scattered angle is θ_s, and the scattered azimuthal angle is ϕ_s. The polarization direction is rotated counterclockwise by the angle α (i.e., polarization angle) from e_θ within the incidence plane. The 2-D Gaussian randomly rough surface is simulated by the Monte Carlo method [15], and the Gaussian power spectral density function is written

$$W(K_{xm}, K_{yn}) = \frac{l_x l_y h^2}{4\pi} \exp\left(-\frac{K_{xm}^2 l_x^2}{4} - \frac{K_{yn}^2 l_y^2}{4}\right) \qquad (1)$$

In Equation (1), h is the root mean square (rms) of 2-D random surface height, and l_x and l_y are the correlation lengths along the x- and y-directions. For convenience, let $l_x = l_y = l$ in this study.

In Figure 2, the domain $ABCDEFGH$ is the computation space and is truncated by uniaxial perfectly matched layer (UPML) [16] for absorbing the outward-propagating waves. For the sake of simplicity, the UPML regions are not specifically plotted in Figure 2(a). The incident plane wave is generated on the connective boundary (i.e., the interface $E'F'G'H'$). In addition, the output boundary (i.e., the interface $A'B'C'D'$) must be set to do a near-to-far transformation. The tangent plane along x direction is illustrated in Figure 2(b).
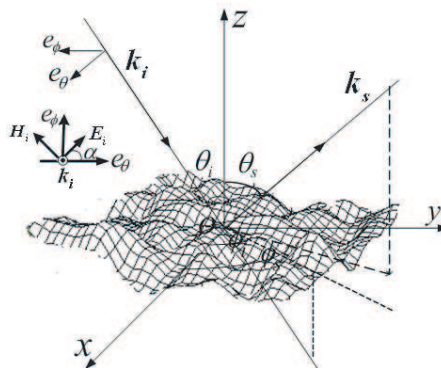
Figure 1. Geometry of incident wave and scattered wave in the coordinate xyz.
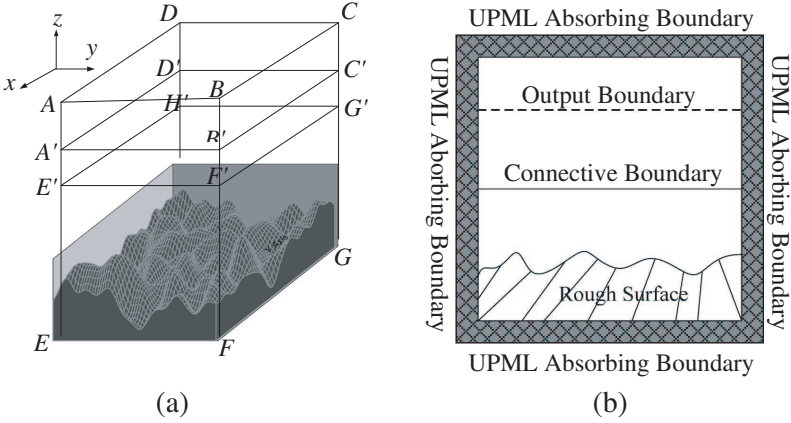
Figure 2. A FDTD model of 2-D rough surface.

2.1. Computation of Near Fields

It is assumed that the 2-D nondispersive rough surface is investigated in the paper, and the complex relative permittivity of rough surface is a constant. For the x components of electric- and magnetic-field, the finite-difference equations are expressed as [17]

$$
E_x^{n+1}\left(i+\frac{1}{2}, j, k\right) = CA\left(i+\frac{1}{2}, j, k\right) E_x^n\left(i+\frac{1}{2}, j, k\right) + CB\left(i+\frac{1}{2}, j, k\right)
$$

$$
\left[\frac{H_z^{n+1/2}\left(i+\frac{1}{2}, j+\frac{1}{2}, k\right) - H_z^{n+1/2}\left(i+\frac{1}{2}, j-\frac{1}{2}, k\right)}{\Delta y}\right.
$$

$$
\left. - \frac{H_y^{n+1/2}\left(i+\frac{1}{2}, j, k+\frac{1}{2}\right) - H_y^{n+1/2}\left(i+\frac{1}{2}, j, k-\frac{1}{2}\right)}{\Delta z}\right] \tag{2}
$$

$$
H_x^{n+\frac{1}{2}}\left(i, j+\frac{1}{2}, k+\frac{1}{2}\right) = CP\left(i, j+\frac{1}{2}, k+\frac{1}{2}\right) \cdot H_x^{n-\frac{1}{2}}\left(i, j+\frac{1}{2}, k+\frac{1}{2}\right)
$$

$$
-CQ\left(i, j+\frac{1}{2}, k+\frac{1}{2}\right) \cdot \left[\frac{E_z^n\left(i, j+1, k+\frac{1}{2}\right) - E_z^n\left(i, j, k+\frac{1}{2}\right)}{\Delta y}\right.
$$

$$
\left. - \frac{E_y^n\left(i, j+\frac{1}{2}, k+1\right) - E_y^n\left(i, j+\frac{1}{2}, k\right)}{\Delta z}\right] \tag{3}
$$

In Equations (2)–(3), i, j and k are the integers. The coefficients CA, CB, CP, CQ are related to the electrical permittivity ε, the

magnetic permeability μ, the electric conductivity σ, and the magnetic conductivity σ_m [17]. Δx, Δy and Δz are the spatial increments in the x-, y- and z-directions, and Δt is the time increment. To ensure the stability and accuracy of the FDTD algorithm [18], the Courant stability limit in this paper could be set as $\Delta x = \Delta y = \Delta z = \Delta$, $\Delta t = 0.5 \times \Delta/c$, and c is the light speed propagation in the vacuum. Similarly, finite-difference approximations for the y- and z-components can be similarly derived as shown by Ref. [17].

The Equations (2)–(3) can been used for the calculation of the whole computation domain except for the connective boundary and the absorbing boundary. The incident plane wave is generated on the interface $E'F'G'H'$ and limited in the total region using a total/scattered field formulation [17]. The sinusoidal excitation source in steady state is expressed as

$$E_i = \begin{cases} 0 & t < 0 \\ E_0 \sin(\omega t) & t \geq 0 \end{cases} \qquad (4)$$

In Equation (4), E_0 is the amplitude of E_i. To reduce the time taken to reach a steady state, the incident wave E_i could be multiplied by a switch function. Where the raised cosine function is adopted

$$U = \begin{cases} 0 & t < 0 \\ 0.5[1 - \cos(\pi t/t_0)] & 0 \leq t < t_0 \\ 1 & t_0 \leq t \end{cases} \qquad (5)$$

where t_0 is a time constant. And in the study, $t_0 = T_0/2$, T_0 is the period of sinusoidal wave source. Where the use of U is not physical and only speeds up the foundation of steady state.

The Gaussian pulse wave in transient scattering is given by

$$e_i = \exp\left(-4\pi(t - t_0)^2/\tau^2\right) \qquad (6)$$

In numerical simulations, finite-length rough surface must be used to model scattering from infinite rough surface. When a plane wave strikes a finite-length rough surface, the reflection at the edge of connective boundary occur. One way of minimizing reflection is to construct an incident wave that tapers to very small values at the edges of the interface $E'F'G'H'$. Reflection still occurs, but it makes negligible contributions to the scattered field. To solve this problem, Fung et al. [19] put forward the Gauss window function to suppress the truncation effect.

2.2. Computation of Far Fields

To obtain the far zone scattered characteristic of 2-D rough surface, it is necessary to implement an near zone to far zone transformation on

the interface $A'B'C'D'$. In terms of the surface equivalence theorem, the scattered electric field in far zone are given by [17]

$$\mathbf{E}^s = -\nabla \times \mathbf{F} - \mathrm{j}\omega\mu_0\mathbf{A} - \mathrm{j}\omega\varepsilon_0\nabla(\nabla \cdot \mathbf{A}) \tag{7}$$

where $\mathrm{j} = \sqrt{-1}$, ε_0 and μ_0 are the electrical permittivity and the magnetic permeability in vacuum. $\mathbf{A}$ and $\mathbf{F}$ are the vector potential functions and written as

$$\mathbf{A}(\mathbf{r}) = \int \mathbf{J}(\mathbf{r}')G(\mathbf{r}, \mathbf{r}')ds' \tag{8}$$

$$\mathbf{F}(\mathbf{r}) = \int \mathbf{J}_m(\mathbf{r}')G(\mathbf{r}, \mathbf{r}')ds' \tag{9}$$

In Equations (8) and (9), $\mathbf{J}$ and $\mathbf{J}_m$ are the equivalent surface electric current and magnetic current, respectively. $G(\mathbf{r}, \mathbf{r}')$ is the 3-D Green's function of free space. $\mathbf{r}$ is the point of observation, and $\mathbf{r}'$ is the source point on the surface ds'.

In terms of the sinusoidal FDTD, an extrapolation from near zone to far zone is not carried out until the computation run reaches to the steady state. Put the observation point $\mathbf{r}$ in the far field and the expressions (8)–(9) become

$$\mathbf{A}(\mathbf{r}) = \frac{\exp(-\mathrm{j}kr)}{4\pi r} \int \mathbf{J}(\mathbf{r}') \exp(\mathrm{j}k\mathbf{r}' \cdot \mathbf{e_r}) \, ds' \tag{10}$$

$$\mathbf{F}(\mathbf{r}) = \frac{\exp(-\mathrm{j}kr)}{4\pi r} \int \mathbf{J}_m(\mathbf{r}') \exp(\mathrm{j}k\mathbf{r}' \cdot \mathbf{e_r}) \, ds' \tag{11}$$

where k is the incident wavenumber, $\mathbf{e_r}$ is the unit vector of $\mathbf{r}$, and $r = |\mathbf{r}|$. Substituting the Equations (10) and (11) into the Equation (7), we obtain [20]

$$\begin{cases} E_\theta^s = -\mathrm{j}kF_\phi - \mathrm{j}\omega\mu_0 A_\theta \\ E_\phi^s = \mathrm{j}kF_\theta - \mathrm{j}\omega\mu_0 A_\phi \end{cases} \tag{12}$$

In the paper, we choose the incident plane xoz (see Figure 1) as the reference plane. Thus the horizontal polarization wave is incident on a 2-D rough surface if the incident electric field is in the plane xoz (i.e., $\alpha = 0°$). Otherwise, the vertical polarization wave is considered (i.e., $\alpha = 90°$). And the normalized radar cross section (i.e., RCS per unit area) in the far zone is defined as [21].

$$\sigma_{\mathrm{HH}} = \lim_{r\to\infty} \frac{4\pi r^2}{S} \frac{|E_\theta^s|^2}{|E_i|^2} \quad \sigma_{\mathrm{VH}} = \lim_{r\to\infty} \frac{4\pi r^2}{S} \frac{|E_\phi^s|^2}{|E_i|^2} \quad \alpha = 0° \tag{13a}$$

$$\sigma_{\mathrm{HV}} = \lim_{r\to\infty} \frac{4\pi r^2}{S} \frac{|E_\theta^s|^2}{|E_i|^2} \quad \sigma_{\mathrm{VV}} = \lim_{r\to\infty} \frac{4\pi r^2}{S} \frac{|E_\phi^s|^2}{|E_i|^2} \quad \alpha = 90° \tag{13b}$$

where S is the area of 2-D rough surface.

Different from the sinusoidal FDTD, the solution of pulsed FDTD is to perform an FDTD calculation and use the currently calculated data on output boundary to extrapolate to the far field. That is to say, for the pulsed FDTD the extrapolation is implemented at every time step. But the extrapolation approach of pulsed FDTD is related to that of sinusoidal FDTD. We can rewrite the Equation (12) as

$$\begin{cases} E_\theta^s = -jk(\eta_0 A_\theta + F_\phi) = -(\eta_0 W_\theta + U_\phi) \\ E_\phi^s = -jk(\eta_0 A_\phi - F_\theta) = -(\eta_0 W_\phi - U_\theta) \end{cases} \tag{14}$$

where η_0 is the wave impedance in free space. W_θ, W_ϕ, U_θ and U_ϕ are the components of the vectors $\mathbf{W}$ and $\mathbf{U}$.

$$\mathbf{W} = jk\mathbf{A}(\mathbf{r}) = jk\frac{\exp(-jkr)}{4\pi r} \int \mathbf{J}(\mathbf{r}') \exp(jk\mathbf{r}' \cdot \mathbf{e_r}) \, ds' \tag{15}$$

$$\mathbf{U} = jk\mathbf{F}(\mathbf{r}) = jk\frac{\exp(-jkr)}{4\pi r} \int \mathbf{J}_m(\mathbf{r}') \exp(jk\mathbf{r}' \cdot \mathbf{e_r}) \, ds' \tag{16}$$

Taking the inverse Fourier transform of the Equations (14), (15) and (16), we obtain

$$\begin{cases} e_\theta^s = -u_\phi - \eta_0 w_\theta \\ e_\phi^s = u_\theta - \eta_0 w_\phi \end{cases} \tag{17}$$

$$\mathbf{w} = \frac{1}{4\pi rc} \frac{\partial}{\partial t} \int \mathbf{j}\left(\mathbf{r}', t + \frac{\mathbf{e_r} \cdot \mathbf{r}'}{c} - \frac{r}{c}\right) ds' \tag{18}$$

$$\mathbf{u} = \frac{1}{4\pi rc} \frac{\partial}{\partial t} \int \mathbf{j_m}\left(\mathbf{r}', t + \frac{\mathbf{e_r} \cdot \mathbf{r}'}{c} - \frac{r}{c}\right) ds' \tag{19}$$

In the Equations (18) and (19), $\mathbf{j}$ and $\mathbf{j_m}$ are the time-domain electric and magnetic scattered surface currents on the interface $A'B'C'D'$. e_θ^s and e_ϕ^s are the time-domain far zone scattered fields. Now the key point is the solution of $\mathbf{w}$ and $\mathbf{u}$, referring to [20]. Transforming e_θ^s, e_ϕ^s and e_i in Equation (6) to E_θ^s, E_ϕ^s and E_i by Fourier transform, and substituting E_θ^s, E_ϕ^s and E_i into the Equations (13a) and (13b), we can obtain the frequency response of 2-D rough surface.

2.3. MPI-based Parallel FDTD Algorithm

In practical FDTD computation, the number of unknowns and the memory cost become extremely larger with the increase of rough surface size. So it is necessary to seek a technique to improve computation efficiency. Fortunately, in FDTD updating, the calculation of electric field value depends only on its four nearest magnetic field values obtained a half time step before.

The same statement is true for the magnetic field calculation. Therefore, the FDTD method is parallel in nature. In this section, the parallel-processing FDTD technique using the Message-Passing Interface (MPI) library [14, 22] is introduced simply. And this parallel workstation is composed of some PC clusters with the same performance, which are connected by internet each other. The main performance of PC clusters is as follows:

1) For each PC CPU: Intel Pentium 4, 3.0 GHz; Memory: 1 GB; Main-board: ASUS P5KSE;

2) Switch: TP-Link TL-R402M 1000M;

3) Operation system: Windows XP;

4) Programming environment: MPICH2, Visual Fortran.

It is important for improving the parallel efficiency to design comfortably a scheme to exchange the field information from one process to another. In terms of 2-D rough surface, the value in the z direction denotes the profile of rough surface. So the number of cell in the z direction is much less that in the x and y directions. And it is improper to divide the computation domain along the x-y plane to achieve the minimum information exchange with its neighbors. In addition, to reduce the amount of communications as much as possible, the location of the subdomain boundary should be arranged properly. Where the values on the boundary region, which is one-cell wide, are shared by the two neighboring tasks. For the sake of simplicity, we assume that the processes are placed along the x direction. In Figure 3, at each time step only the tangential magnetic fields H_y and H_z are exchanged between neighbor tasks, and the tangential electric fields E_y and E_z on the actual subdomain interface will become the inner points, and will be independently calculated in their own processes. Another significant advantage of this approach is that the mesh and material information for the electric-field update has already been included in its own subdomain.

3. NUMERICAL RESULTS

In what follows, the numerical results of the polarimetric scattering from 2-D rough surface with sinusoidal and pulsed wave excitation for different conditions are presented and discussed in detail. Where the highest frequency in pulsed FDTD is equal to 0.3 GHz (i.e., the wavelength $\lambda_{\min} = 1.0$ m). The size of rough surface is $S = 51.2 \times 51.2$ m^2, the spatial increment is taken as $\Delta x = \Delta y = \Delta z = \Delta = 0.1$ m, and the UPML thickness is 5Δ. The electrical permittivity and the electric conductivity are $\varepsilon = 2.5\epsilon_0$ and $\sigma = 2\pi f \varepsilon_0$ ($f = 0.3$ GHz),
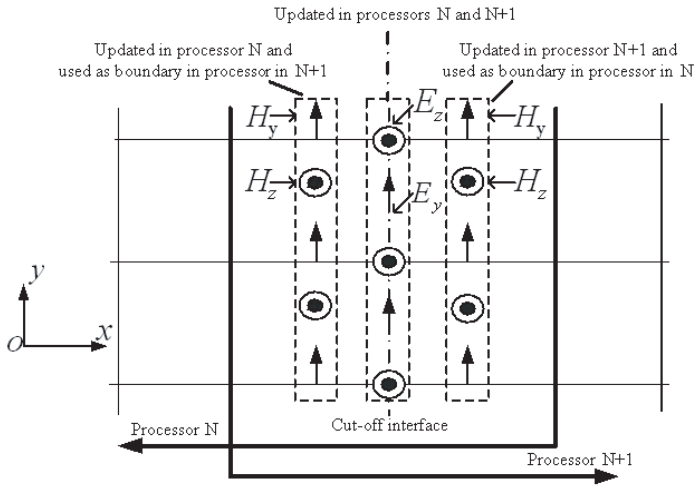
Figure 3. Boundary region of adjacent processors in the FDTD method.

respectively. As far as the pulsed incident wave is concerned, $\tau = 60\Delta t$ and $t_0 = 0.8\tau$ in the Equation (6). For convenience, some parameters for describing the rough surface in sinusoidal FDTD calculation are measured in wave length λ. And the incident azimuthal angle is $\phi_i = 180°$ and the 2-D rough surface is averaged by 10 Monte Carlo realizations in the following numerical results.

3.1. Validation

In order to ensure the validity of FDTD algorithm presented in the paper, in Figure 4 we firstly compute the angular distribution of bistatic scattering coefficient from 2-D PEC and dielectric rough surface ($h = 0.1\lambda$, $l_x = l_y = 1.0\lambda$) using sinusoidal FDTD method and the Kirchhoff Approximation (KA) [23], respectively. Where the incident angle is $20°$, and the bistatic HH-polarized scattering is considered. It is obvious that the angular distribution of scattering coefficient for both PEC (Figure 4(a)) and dielectric (Figure 4(b)) rough surface by sinusoidal FDTD is in good agreement with that obtained by KA except for the large scattering angles, which demonstrates the feasibility and applicability of sinusoidal FDTD algorithm.

In Figure 5, the NRCS from 2-D Gaussian rough surface versus frequency by the pulsed FDTD method for different conditions is plotted in Figure 5 by solid line. And the numerical result by the
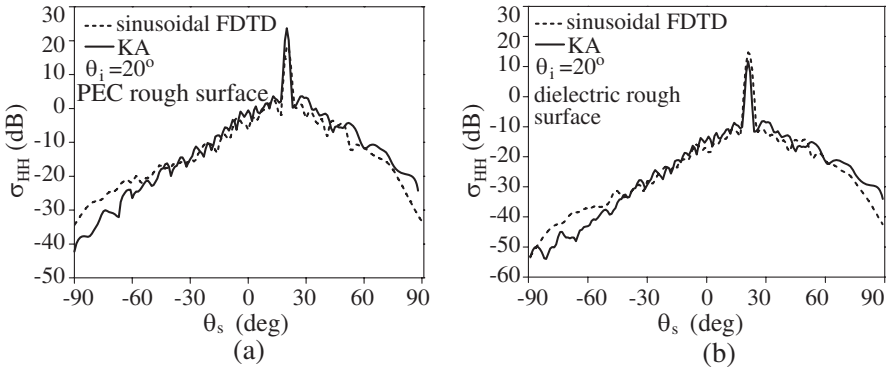
Figure 4. Sinusoidal FDTD method and KA method for the NRCS from 2-D rough surface versus scattered angle, $\theta_i = 20°$, (a) PEC rough surface, (b) dielectric rough surface.
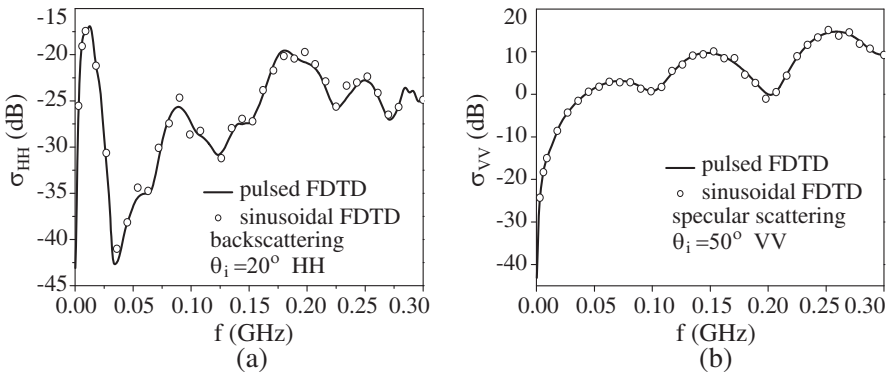

Figure 5. Pulsed FDTD and sinusoidal FDTD for the NRCS from 2-D rough surface versus frequency, (a) HH $\theta_i = 20°$, (b) VV $\theta_i = 50°$.

sinusoidal FDTD method is also shown by circle for the comparison. For the sinusoidal FDTD method, the NRCS for each frequency needs an individual FDTD run, but adopting the pulsed FDTD method can obtain results over a wide frequency band from a single FDTD run. It should be noted that the modeling requirements (cell size and model size) for the sinusoidal FDTD are identical to those required for the highest frequency in pulsed FDTD. Since the electrical properties of rough surface to be modeled are identical, the physical models are identical for pulsed FDTD and sinusoidal FDTD. Where the rms height and the correlation length of Gaussian rough surface are $h = 0.15\,\mathrm{m}$ and $l_x = l_y = 1.0\,\mathrm{m}$, respectively. Figure 5(a) shows the wide-band

backscattering for the HH polarization, and Figure 5(b) is the result of specular scattering for the VV polarization. It is easily observed that the numerical results by sinusoidal FDTD agree well with that of pulsed FDTD in Figure 5. This indicates the validity of our FDTD method with pulsed wave excitation.

3.2. Analysis of Parallel Computation

For the purpose of comparing the performance of parallel algorithm shown in the paper, taking sinusoidal FDTD for example, the bistatic scattering from the 2-D rough surface ($h = 0.1\lambda$, $l_x = l_y = 1.0\lambda$) with VV polarization for different processes along the y direction are investigated in the following. The incident angle is $30°$, and a computation domain of $512 \times 512 \times 30$ cells is considered. Figure 6(a) presents the angular distribution of NRCS from one rough surface realization, and for convenience only the results from series FDTD and 8-process parallel FDTD are compared. It is obvious that the scattering results obtained using series FDTD and parallel FDTD overlay each other exactly over the whole scattered angular range. The computation time from only one rough surface for different processes is presented in Table 1. It is seen that the time cost reduces dramatically with the increasing of the number of process.
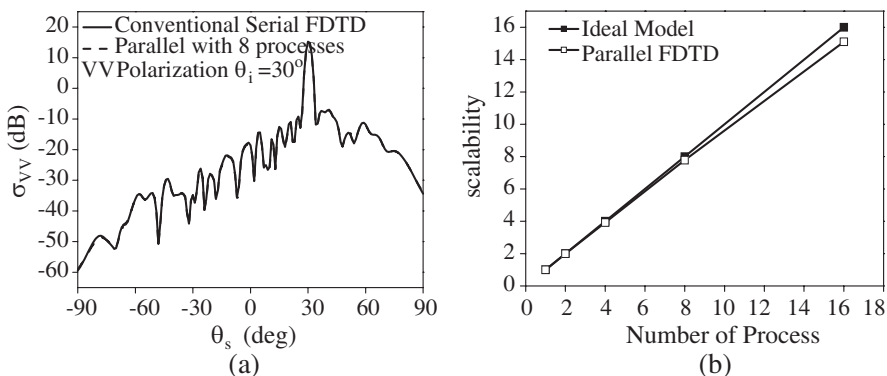
Figure 6. (a) NRCS from one rough surface realization for different processes. (b) Scalability of parallel FDTD algorithm for different processes.

Figure 6(b) investigates the scalability [14] of parallel sinusoidal FDTD algorithm for different processes. It is readily found that the parallel scalability is almost linearly proportion to the numbers of processes involved in the computing parallel system. Another point worth mentioning is that the scalability of parallel FDTD is far from

Table 1. Comparison of time with one rough surface realization for different.

| Processes	1	2	4	8	16
Time	22447.80 s	11280.30 s	5726.48 s	2285.32 s	1486.61 s

that of the ideal model due to the larger communication time with the increase of the number of process.

It should be pointed out that 16-process parallel algorithm is adopted in the following sinusoidal FDTD and pulsed FDTD.

3.3. Analysis of NRCS

In Figure 7, the angular distribution of NRCS from 2-D Gaussian rough surface ($h = 0.1\lambda$, $l_x = l_y = 1.0\lambda$) are shown for the different polarizations. It is clear that the co-polarized (HH and VV) scattering from rough surface is much stronger than the cross-polarized (VH and HV) scattering over the whole scattered angular range for incident angle 40° (Figure 7(a)) and incident angle 50° (Figure 7(b)). And the scattering peaks are obvious in specular direction for co-polarized scattering. In addition, it is not difficultly found that the difference between the VV polarization and HH polarization can been distinguished when the scattering angle is larger than that of the specluar direction, and in these scattering direction the result from VV polarization is stronger than that of HH polarization.

The NRCS from the 2-D rough surface versus the frequency in
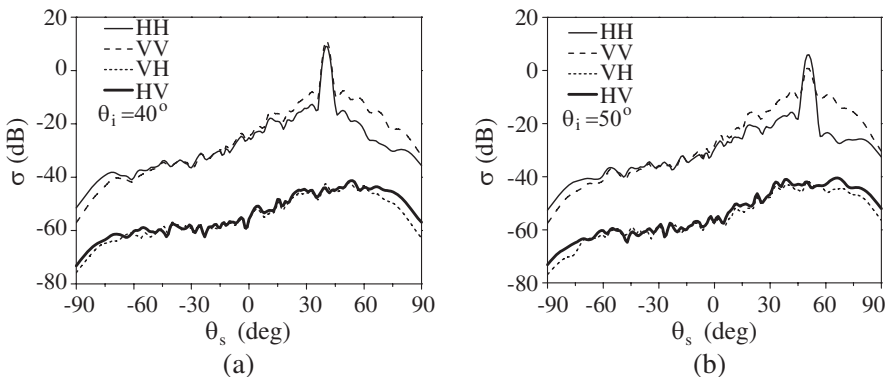
Figure 7. NRCS from 2-D rough surface for different polarizations, (a) $\theta_i = 40°$, (b) $\theta_i = 50°$.
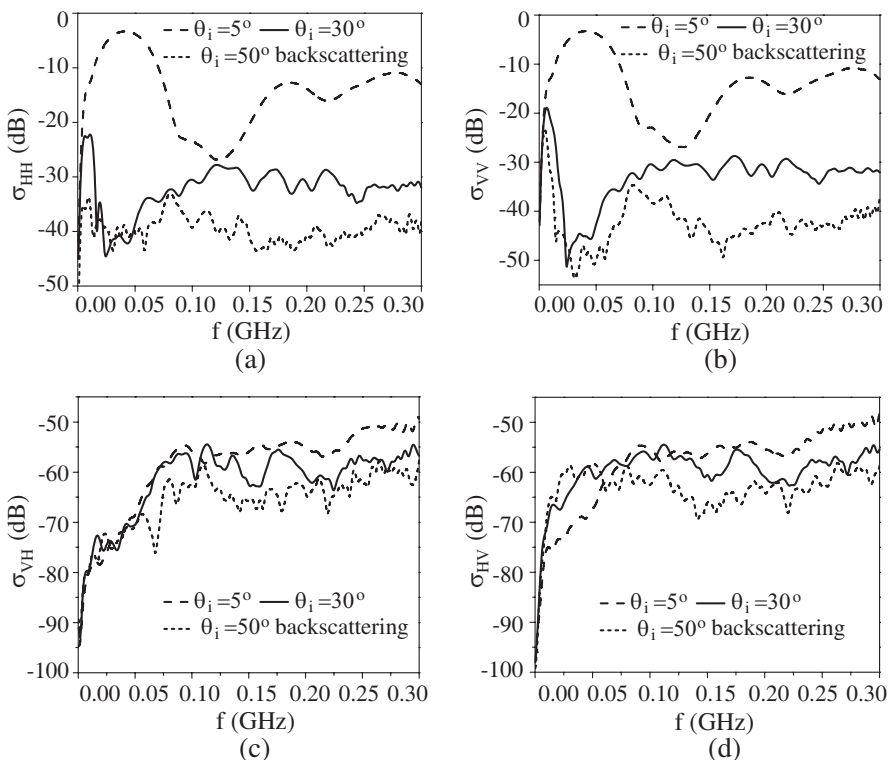
Figure 8. NRCS from 2-D rough surface versus frequency for different incident angles, (a) HH polarization, (b) VV polarization, (c)VH polarization, (d) HV polarization.

the backward direction for different incident angles is analyzed in the Figure 8. The rms height and the correlation length of rough surface are 0.1 m and 1.0 m, respectively. And the electromagnetic parameters of rough surface are the same as those in Figure 5. It is obvious that the NRCS of rough surface become smaller with the increase of the incident angle for all the polarizations. In addition, for the same incident angle, the co-polarized (Figures 8(a)–(b)) NRCS is much larger than that of the cross polarizations(Figures 8(c)–(d)), which is similar to that of sinusoidal FDTD in Figure 7.

4. CONCLUSION

FDTD algorithm with sinusoidal and pulsed plane wave excitations is adopted to investigate the polarimetric scattering of 2-D Gaussian

rough surface. The basic theory of the far zone scattered field calculated by sinusoidal FDTD and pulsed FDTD is presented. And the parallel technique based on MPI library is also introduced to speed up the computation efficiency. The NRCS from 2-D rough surface in various directions by sinusoidal FDTD method is compared with the results by KA method. And The NRCS of 2-D rough surface versus frequency in the backward and specular directions by pulsed FDTD method is also compared with that obtained by sinusoidal FDTD method. Good agreement is observed for all cases, which denotes the validity of present FDTD method. Finally, the complete polarimetric scattering characteristic of rough surface by sinusoidal and pulsed FDTD is presented and analyzed for different polarizations in detail. Future investigation will include the composite scattering from the arbitrary 3-D target and 2-D rough surface using the FDTD technique.

ACKNOWLEDGMENT

REFERENCES

1. Bourlier, C., "Azimuthal harmonic coefficients of the microwave backscattering from a non-Gaussian ocean surface with the first-order SSA model," *IEEE Trans. Geosci. Remote Sensing*, Vol. 42, No. 11, 2600–2611, 2004.

2. Cocheril, Y. and R. Vauzelle, "A new ray-tracing based wave propagation model including rough surfaces scattering," *Progress In Electromagnetics Research*, PIER 75, 357–381, 2007.

3. Guo, L. X. and Z. S. Wu, "Application of the extended boundary condition method to electromagnetic scattering from rough dielectric fractal sea surface," *Journal of Electromagnetic Waves and Applications*, Vol. 18, No. 9, 1219–1234, 2004.

4. Torrungrueng, D., H. T. Chou, and J. T. Johnson, " A novel acceleration algorithm for the computation of scattering from two-dimensional large-scale perfectly conducting random rough surfaces with the forward-backward method," *IEEE Trans. Geosci. Remote Sensing*, Vol. 38, No. 4, 1656–1668, 2000.

5. Jandhyala, V., E. Michielssen, S. Balasubramaniam, and W. C. Chew, "A combined steepest descent-fast multipole algorithm for the fast analysis of three-dimensional scattering by rough surfaces," *IEEE Trans. Geosci. Remote Sens.*, Vol. 36, No. 3, 738–748, 1998.

6. Xia, M. Y., C. H. Chan, S. Q. Li, B. Zhang, and L. Tsang, "An efficient algorithm for electromagnetic scattering from rough surfaces using a single integral equation and multilevel sparse-matrix canonical-grid method," *IEEE Trans. Antennas Propagat.*, Vol. 51, No. 6, 1142–1149, 2003.

7. Lesha, M. J. and F. J. Paoloni, " Transient scattering from arbitrary conducting surfaces by iterative solution of the electric field integral equation," *Journal of Electromagnetic Waves and Applications*, Vol. 10, No. 8, 1139–1167, 1996.

8. Johnson, J. T. and R. J. Burkholder, "A study of scattering from an object below a rough surface," *IEEE Trans. Geosci. Remote Sens.*, Vol. 42, No. 1, 59–66, 2004.

9. Li, J., L. X. Guo, H. Zeng, and X..B. Han, "Message-passing-interface-based parallel FDTD investigation on the EM scattering from a 1-D rough sea surface using uniaxial perfectly matched layer absorbing boundary," *J. Opt. Soc. Am. A.*, Vol. 26, No. 6, 1494–1502, 2009.

10. Li, J., L. X. Guo, and H. Zeng, "FDTD investigation on bistatic scattering from two-dimensional rough surface with UPML absorbing condition," *Waves in Random and Complex Media*, Vol. 19, No. 3, 418–429, 2009.

11. Li, J., L. X. Guo, and H. Zeng, "FDTD investigation on the electromagnetic scattering from a target above a randomly rough a sea surface," *Waves in Random and Complex Media*, Vol. 18, No. 4, 641–650, 2008.

12. Guo, L. X., J. Li, and H. Zeng, "Bistatic scattering from a three-dimensional object above a two-dimensional randomly rough surface modeled with the parallel FDTD approach," *J. Opt. Soc. Am. A.*, Vol. 26, No. 11, 2383–2392, 2009.

13. Li, J., L. X. Guo, and H. Zeng, "FDTD investigation on bistatic scattering from a target above two-layered rough surfaces using UPML absorbing condition," *Progress In Electromagnetics Research*, PIER 88, 197–211, 2008.

14. Guiffaut, C. and K. Mahdjoubi, "A parallel FDTD algorithm using the MPI library," *IEEE Antennas and Propagation Magazine*, Vol. 43, No. 2, 94–103, 2001.

15. Kuga, Y. and P. Phu, "Experimental studies of millimeter wave

scattering in discrete random media and from rough surfaces,"
Progress In Electromagnetics Research, PIER 14, 37–88, 1996.

16. Gedney, S. D., "An anisotropic PML absorbing media for the
FDTD simulation for fields in lossy and dispersive media,"
Electromagnetics, Vol. 16, No. 4, 425–449, 1996.

17. Taflove, A. and S. C. Hagness, *Computational Electrodynamics:
The Finite-difference Time-domain Method*, Artech House,
Norwood, 2005.

18. Juntunen, J. S. and T. D. Tsiboukis, "Reduction of numerical
dispersion in FDTD method through artificial anisotropy," *IEEE
Trans. Microwave Theory Tech.*, Vol. 58, No. 5, 582–588, 2000.

19. Fung, A. K., M. R. Shah, and S. Tjuatja, "Numerical simulation
of scattering from three-dimensional randomly rough surfaces,"
IEEE Trans. Geosci. Remote Sensing, Vol. 32, No. 5, 986–995,
1994.

20. Luebbers, R. J., K. S. Kunz, M. Schneider, and F. Hunsberger,
"A finite-difference time-domain near zone to far zone transforma-
tion," *IEEE Trans. Antennas Propagat.*, Vol. 39, No. 4, 429–433,
1991.

21. Kong, J. A., *Electromagnetic Wave Theory*, Wiley, New York,
1986.

22. Yu, W. H., Y. J. Liu, T. Su, N. T. Hunag, and R. Mittra, "A
robust parallel conformal finitedifference time-domain processing
package using the MPI library," *IEEE Antennas and Propagation
Magazine*, Vol. 47, No. 3, 39–59, 2005.

23. Ogilvy, J. A., *Theory of Wave Scattering from Random Rough
Surface*, IOP Publishing, 1991.